UC Irvine
UC Irvine Previously Published Works

Title
Model study of tropospheric trace species distributions during PEM-West A

Permalink
https://escholarship.org/uc/item/97b279fp

Journal
Journal of Geophysical Research, 101(D1)

ISSN
0148-0227

Authors
Liu, SC
McKeen, SA
Hsie, E-Y
et al.

Publication Date
1996-01-20

DOI
10.1029/95jd02277

Copyright Information
This work is made available under the terms of a Creative Commons Attribution License, availalbe at https://creativecommons.org/licenses/by/4.0/

Peer reviewed

eScholarship.org Powered by the California Digital Library
University of California

JOURNAL OF GEOPHYSICAL RESEARCH, VOL. 101, NO. D1, PAGES 2073–2085, JANUARY 20, 1996

Model study of tropospheric trace species distributions during PEM-West A

S. C. Liu,[1] S. A. McKeen,[1,2] E-Y. Hsie,[1,2] X. Lin,[1,2] K. K. Kelly,[1] J. D. Bradshaw,[3] S. T. Sandholm,[3] E. V. Browell,[4] G. L. Gregory,[4] G. W. Sachse,[4] A. R. Bandy,[5] D. C. Thornton,[5] D. R. Blake,[6] F. S. Rowland,[6] R. Newell,[7] B. G. Heikes,[8] H. Singh,[9] and R. W. Talbot[10]

Abstract. A three-dimensional mesoscale transport/photochemical model is used to study the transport and photochemical transformation of trace species over eastern Asia and western Pacific for the period from September 20 to October 6, 1991, of the Pacific Exploratory Mission-West A experiment. The influence of emissions from the continental boundary layer that was evident in the observed trace species distributions in the lower troposphere over the ocean is well simulated by the model. In the upper troposphere, species such as O_3, NO_y (total reactive nitrogen species), and SO_2 which have a significant source in the stratosphere are also simulated well in the model, suggesting that the upper tropospheric abundances of these species are strongly influenced by stratospheric fluxes and upper tropospheric sources. In the case of SO_2 the stratospheric flux is identified to be mostly from the Mount Pinatubo eruption. Concentrations in the upper troposphere for species such as CO and hydrocarbons, which are emitted in the continental boundary layer and have a sink in the troposphere, are significantly underestimated by the model. Two factors have been identified to contribute significantly to the underestimate: one is emissions upwind of the model domain (eastern Asia and western Pacific); the other is that vertical transport is underestimated in the model. Model results are also grouped by back trajectories to study the contrast between compositions of marine and continental air masses. The model-calculated altitude profiles of trace species in continental and marine air masses are found to be qualitatively consistent with observations. However, the difference in the median values of trace species between continental air and marine air is about twice as large for the observed values as for model results. This suggests that the model underestimates the outflow fluxes of trace species from the Asian continent and the Pacific rim countries to the ocean. Observed altitude profiles for species like CO and hydrocarbons show a negative gradient in continental air and a positive gradient in marine air. A mechanism which may be responsible for the altitude gradients is proposed.

1. Introduction

As stated in the overview paper by *Hoell et al.* [this issue], a major objective of the Pacific Exploratory Mission (PEM-West) campaign is to evaluate the anthropogenic impact on the distributions of trace gases and aerosols over the western Pacific basin, particularly those associated with O_3, O_3 precursors, and sulfur species. A number of papers in this special issue have addressed this subject by analyzing data obtained during the campaign [e.g., *Gregory et al.*, this issue; *Smyth et al.*, this issue; *Talbot et al.*, this issue]. In this paper we will study this subject from the model perspective.

We use a three-dimensional mesoscale model that covers eastern Asia and the western Pacific (Figure 1a) to simulate the transport and photochemical transformation of trace species for the period from September 20 to October 6, 1991, when the DC-8 made intensive observations over the western Pacific from Yokota, Japan, Hong Kong, and Guam [*Hoell et al.*, this issue]. A brief discussion of the model, its initial and boundary conditions, and emission inventories is given in section 1.

To get a general idea of how well the model simulates the atmosphere, spatial distributions of trace species calculated by the model are first compared directly to observations. Latitude-longitude distributions for some key species in the boundary layer and in the upper troposphere from model results are plotted and compared to the aircraft measurements. Model results are also grouped by back trajectories to study the contrast between the composition of marine and continental air and to compare with similar analyses that were applied to observations by *Gregory et al.* [this issue] and *Talbot et al.* [this issue]. In the comparison, emphasis will be placed on the altitude profiles of continental and marine air masses. We expect a reasonably good agreement between the gross fea-

[1]Aeronomy Laboratory/NOAA, Boulder, Colorado.
[2]Cooperative Institute for Research in Environmental Sciences, University of Colorado, Boulder.
[3]Georgia Institute of Technology, Atlanta.
[4]NASA Langley Research Center, Hampton, Virginia.
[5]Drexel University, Philadelphia, Pennsylvania.
[6]University of California, Irvine.
[7]MIT, Cambridge, Massachusetts.
[8]University of Rhode Island, Narragansett.
[9]NASA Ames Research Center, Moffett Field, California.
[10]University of New Hampshire, Durham.

Copyright 1996 by the American Geophysical Union.

Paper number 95JD02277.
0148-0227/96/95JD-02277$05.00

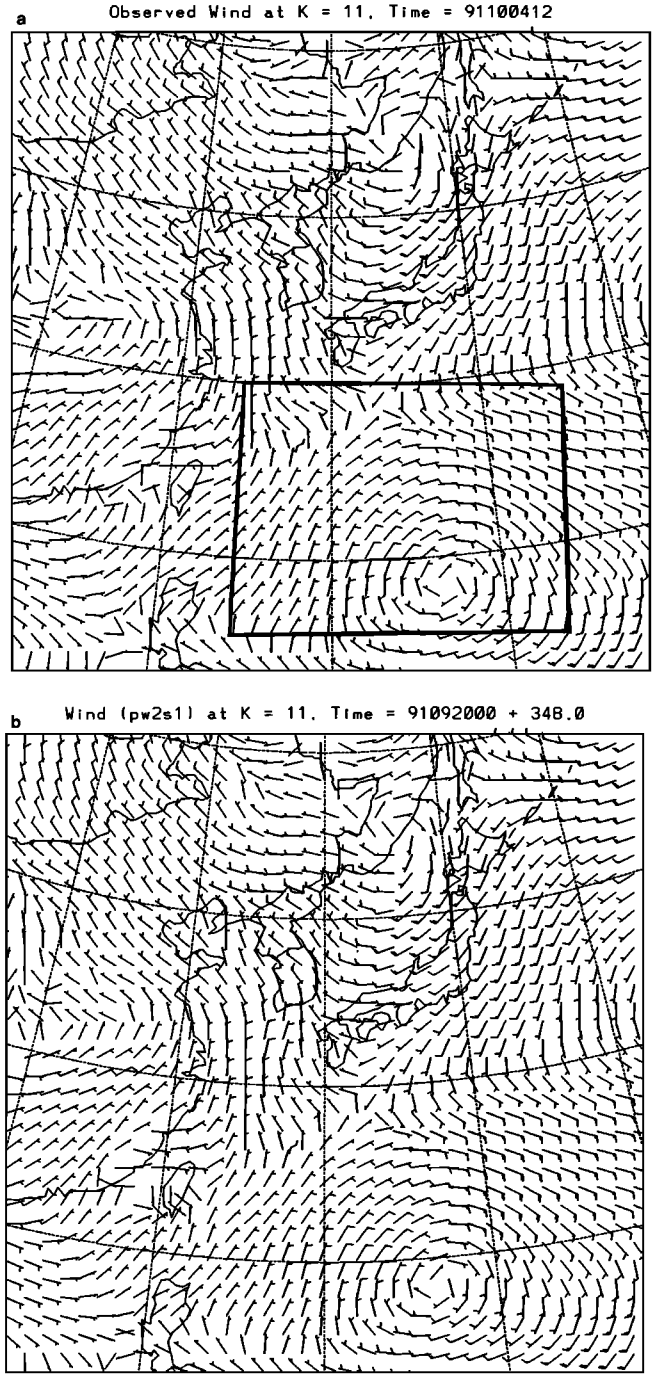

Figure 1. (a) Observed and (b) model-simulated wind fields at eleventh model level (1.15 km) at 1200, October 4, 1991. The square south of Japan in Figure 1a is the study area used for section 3.3.

tures of model results and those of observations, particularly in the lower troposphere. On the other hand, because of the high wind velocity in the upper troposphere the model results tend to be strongly influenced by side boundary conditions [*Brost*, 1988; *McKeen et al.*, 1991]. This problem can be alleviated by substantially increasing the model domain. However, relatively large computer resources are needed for these types of model calculations and will be a subject of future study.

The upper boundary of the model is located near the tropopause. Trace species such as O_3 and NO_y, which have a significant stratospheric source, are modeled by fixing their mixing ratios to values proportional to potential vorticity (PV) at the upper boundary [*Ebel et al.*, 1991]. This allows us to study the budget of NO_y in the upper troposphere, a subject of intensive investigation because of the potential impact of subsonic aircraft emissions on tropospheric O_3 (e.g., NASA report by *Prather et al.* [1992]). During PEM-West A, high concentrations of SO_2 and sulfate were observed in the upper troposphere near stratospheric intrusions on flights 4, 5, and 21. These high values are believed to come from SO_2 injected into the stratosphere by Mount Pinatubo eruptions in June 1991, three months before the mission. Thus we have also looked into the influence of the stratospheric source on the distributions of SO_2 in the upper troposphere by fixing their mixing ratios at values proportional to PV at the upper boundary of the model.

Another emphasis in this paper is to discuss outflow of trace species from the Asian continent and the Pacific rim countries. Implications of the observed altitude profiles of trace gases on the vertical transport over the continent are also examined.

2. Model Description

2.1. Model Structure

A detailed description of the model used in this study can be found in the work of *McKeen et al.* [1991]. The following is a brief description to facilitate discussions below. The model contains two major components: a meteorological/transport model and a photochemical model. The transport model is a three-dimensional, hydrostatic, compressible, primitive-equation model, which is usually called the Penn State/National Center for Atmospheric Research (NCAR) mesoscale model. The version used here is MM4 [*Anthes et al.*, 1987] with four-dimensional data assimilation (FDDA) [*Stauffer and Seaman*, 1991]. The initial and boundary conditions are obtained from the National Meteorological Center (NMC) global data and enhanced by rawinsonde and surface observations. The vertical coordinate of the model is a terrain-following sigma coordinate with the top at 100 mbar. There are 15 vertical layers, and to resolve the boundary layer, half of the layers are concentrated in the lowest 2 km. The photochemical model includes about 35 species and 130 photochemical reactions. Nonmethane hydrocarbons (NMHCs) are included in the model by using the lumped species approach of *Lurmann et al.* [1986].

The data used in the FDDA simulation are 12-hour NMC data enhanced by rawinsonde observations and 3-hour surface observations from NCAR data archives. Both rawinsonde and surface observations are interpolated to the model grids first, then used in the model simulations. Horizontal winds and water vapor mixing ratios are nudged (i.e., FDD-assimilated) throughout the model domain, as suggested by *Stauffer and Seaman* [1991]. Since the model (MM4) is very sensitive to the low-level temperature stratification, nudging of the temperature field is handled differently. Nudging the temperature within model-computed PBL height tends to affect the Blackadar planetary boundary layer (PBL) model drastically. In certain cases we find that the growth of PBL height is delayed by several hours in the morning. Therefore in this study the temperature nudging is only performed above 2 km. Below 2 km we allow the Blackadar PBL scheme to evaluate its own temperature profile. Finally, a parameterized vertical transport

scheme due to convective clouds as described by *Lin et al.* [1994] is included in the model.

In most cases, incorporation of FDDA into MM4 improves the model simulation significantly [*Stauffer and Seaman*, 1991]. For example, we have also made a simulation run of MM4 without FDDA for the PEM-West A period. In this run, neither of the two major typhoons, namely Mireille and Orchid, are fully developed. They stay as tropical depressions. Apparently, the default parameters used in the MM4 cumulus parameterization scheme (Kuo-type scheme) are not suitable for simulating the feedback between frictional convergence and release of latent heat inside the typhoon. The simulation is greatly improved when FDDA is incorporated. Figures 1a and 1b depict the observed and model-simulated wind fields at the eleventh model level (1.15 km) at 1200 UT, October 4, 1991. The synoptic features are very well simulated, including a high-pressure system over northern China (indicated by counterclockwise wind), and a quasi-stationary front is oriented from southwest to northeast from Taiwan to Japan (wind trough). In addition, both the position (18.8°N, 136.7°E) and strength of Typhoon Orchid are in good agreement with observations.

2.2. Emission Inventories

Anthropogenic emissions of NO_x and SO_2 are based on the 1987 country or Chinese province level estimates of *Kato and Akimoto* [1992]. The spatial partitioning within each country or province is taken from the 1° × 1° emission database of *Dignon* [1992] with modifications near coastlines to insure emissions are only over land in the 60 km × 60 km model grid. The only published estimates of anthropogenic hydrocarbons for Asia are those of *Piccot et al.* [1992], which are only available on a 10° × 10° or country resolution. These estimates do not include CO and are lumped into hydrocarbon classes that are not consistent with the *Lurmann et al.* [1986] oxidation mechanism. We have therefore recompiled our own estimates of hydrocarbon and CO emissions in a manner similar to that of *Piccot et al.* [1992] based on fuel use statistics and emission factors relative to NO_x from the U.S. EPA 1985 National Acid Precipitation Assessment Program (NAPAP) emissions inventory [*Environmental Protection Agency* (*EPA*), 1989]. Annual consumption of four fuel types (coal, oil, gas, and vegetative) are available for 31 source categories for individual countries from the World Energy Statistics and Balances 1985–1988 [*Organization for Economic Cooperation and Development/International Energy Association* (*OECD/IEA*), 1990] and the *International Energy Agency* (*IEA*) [1987]. Equivalent fuel use statistics are available for individual Chinese provinces from the Yearbook of Energy Statistics of China 1989 [*State Statistical Bureau of China* (*SSBC*), 1990]. The 350 source classification codes of the EPA NAPAP inventory were then mapped to the 31 source categories and four fuel types within the OECD/IEA reports. Total emissions of NO_x, CO, and hydrocarbons were then calculated for each fuel usage type and source category from the 1985 NAPAP modeler's emission inventory [*EPA*, 1989] to derive average emission ratios relative to NO_x for each of the hydrocarbon classes used in the oxidation mechanism. Hydrocarbon and CO emissions for each model grid are then calculated based on the spatial distribution of the NO_x emissions and the fuel use/source category for each country or province. The net result is a hydrocarbon and CO emissions inventory for Asia that is consistent with the published fuel use statistics for each country or province, the hydrocarbon to NO_x emission ratios of equivalent fuel use in the United States, and the NO_x emissions inventory of *Kato and Akimoto* [1992].

Biogenic emissions of isoprene, monoterpenes, and NO_x are included as a function of land use characteristics within the model domain, which are derived from a global compilation based on the 13 surface categories used within the Penn State/NCAR MM4 model [*Anthes et al.*, 1987]. The natural NMHC emissions are determined in a manner similar to that of *McKeen et al.* [1991] and are based on the estimation method of *Lamb et al.* [1987]. Soil NO_x emissions are included according to *Williams et al.* [1992] with a low emission rate (0.2 ng N m^{-2} s^{-1}) assumed for the agricultural land use category. Thus the effects of fertilization or of biomass burning, other than residential fuel use, are not included in the inventory.

Because there is a large uncertainty in the emission flux of dimethyl sulfite (DMS) during the mission as indicated by the observed large scattering in its mixing ratio in the boundary layer [*Thornton et al.*, this issue], we have omitted DMS emissions in the current model calculations. This will not affect the model-calculated SO_2 concentration significantly as the observed DMS concentrations are very low. Emissions of SO_2 from volcanoes and biomass burning are also omitted because of lack of information on these emissions in the model domain. While these omissions make the emission inventories incomplete, it allows us to test if emissions from Mount Pinatubo and anthropogenic sources can account for the observed abundance of SO_2 in the atmosphere. For the same reason, lightning and subsonic aircraft sources of NO are not included in the current model calculations either. The latter source will be added in future calculations. The lightning source is too uncertain to be included in episodic-type model calculations like ours.

2.3. Initial and Boundary Conditions

The influence of side boundary conditions on a regional model has been well documented by *Brost* [1988] and by *McKeen et al.* [1991]. In the boundary layer the distributions of trace species tend to be controlled by surface emissions and photochemistry within the model domain. At about 2 km the side boundary conditions start to affect significantly the distributions of trace species. Therefore unless the boundary conditions can be accurately defined, substantial errors can occur in the distributions of trace species calculated by the model. As discussed in the introduction, the domain of our model is relatively small. As a result, emissions upwind of the model domain such as those from Europe which are not included in the model have a strong influence on the trace species distributions at the side boundary and thus on those above 2 km within the domain. For this reason, in this paper, we limit most of the discussion of model results to the boundary layer. The only exception is the upper troposphere near the tropopause where the influence of stratospheric intrusions is strong. In this regime we believe that the upper and side boundary conditions are specified reasonably well in the model.

Initial and boundary conditions are applied differently for the bottom 10 levels (0–5 km) and the top 6 levels (5–20 km) of the model domain. To evaluate the impact of anthropogenic emissions on the distributions of trace species, the initial and boundary conditions for the lower portion of the model are chosen to represent clean marine air. At the time when the model calculations first started, only limited preliminary data from the PEM-West A were available. Therefore data from CITE 2 [*Hoell et al.*, 1990] were used to specify the conditions

whenever PEM-West A data were not available. O_3 and CO have latitudinally varying initial and boundary conditions with surface values of 15 and 75 ppbv at the southern boundary, 30 and 120 ppbv at the northern boundary of Figure 1a, respectively. With altitude, O_3 and CO profiles vary exponentially to 9-km values of 53 and 75 ppbv, respectively. Conditions for NO_y below 5 km are taken from the oceanic measurements reported by *Hübler et al.* [1992] for the Chemical Instrumentation Test and Evaluation (CITE 2) experiment, with a linear increase from 105 pptv at the surface to 200 pptv at 5 km uniformly over the model domain. The partitioning of NO_y is also based on CITE 2 oceanic data with $NO_x/NO_y = 0.3$ at 5 km [*Carroll et al.*, 1990] and 0.2 at the surface; $PAN/NO_x = 0.5$, typical of air masses with tropical origins [*Ridley et al.*, 1990]; and with HNO_3 assumed as the remaining fraction of NO_y. SO_2 is initialized as 100 pptv. The initial and boundary conditions for hydrocarbons are specified according to PEM-West A observations; for details the reader is referred to *McKeen et al.* [this issue].

Obviously, the initial and boundary conditions defined above are specified with certain degree of arbitrariness and contain significant uncertainties. As discussed above, when we compare the model results to observations, we will avoid any discussion of the altitude range (about 2 to 6 km) which is affected strongly by the side boundary or initial conditions.

Stratospheric influence on O_3, NO_y, and SO_2 is parameterized by specifying the initial and boundary conditions at the top six altitude levels of the model to values proportional to PV [*Ebel et al.*, 1991]. The proportional coefficients are assumed to be constant. For O_3, 50 ppbv per PV unit is adopted according to the studies by *Ebel et al.* [1991] and *Beekmann et al.* [1994], where the PV unit is 10^{-6} K m^2 kg^{-1} s^{-1}. The proportional coefficient for NO_y is calculated by adopting 4 pptv/ppbv for the ratio of NO_y/O_3 near the tropopause according to *Murphy et al.* [1993]. For SO_2 the proportional coefficient (50 pptv/PV) is derived by making linear fits to the correlation plots of individual species against O_3 for observations during the three flights where O_3, CO, and H_2O displayed a clear indication of stratospheric air above 8 km. The stratospheric influence on CO is also parameterized in a similar manner by fitting a curve through the observed ratio of CO to O_3.

3. Model Results and Comparison With Observations

3.1. Horizontal Distributions of Trace Species

A straight forward display of the contrast between continental and marine air masses can be done by plotting the latitude-longitude distributions at various altitudes for the key species. We will plot these distributions for O_3, NO_y, SO_2, and CO and compare them to observations. These species are chosen because they play important roles in addressing PEM-West objectives. In addition, their distributions are affected by a wide variety of sources, sinks, and photochemical processes so that comparison of their distributions with observed values can be used as a test of the model's capability in simulating those atmospheric processes. For example, among the trace species measured during PEM-West A, CO turns out to be one of the most useful tracers for continental emissions not only because the majority of its sources are located in the continental boundary layer but also because of the large number of observations made by a fast response instrument [*Hoell et al.*, this issue].

When the model results are compared to observations, one important consideration is that while the mesoscale model is expected to simulate the gross features of large meteorological events reasonably well, the exact time and location of each event are not likely to be simulated accurately. We note that large features of the distributions of trace species calculated by the model during the study period do not drastically change with time. Therefore it is more meaningful to compare the time average distributions of the model results with observations rather than making comparisons of simultaneous model results with individual flights. The only obvious exception is the case when Typhoon Mireille brought relatively clean marine air up to the west of Japan and efficiently mixed boundary layer air to the upper troposphere. We will single out and discuss the effects of Typhoon Mireille on trace species distributions in a separate figure. A more detailed discussion of the typhoon and its effects will be presented in another paper by *Newell et al.* [this issue].

Another consideration is to account for the effect that the photochemical lifetime of each species has on its distribution. A species with a long photochemical lifetime relative to the characteristic time of the transport processes in the model domain is expected to have a more uniform distribution than a short-lived species. For example, among the four aforementioned species, CO has the longest photochemical lifetime, about 2 months in the troposphere. Its observed mixing ratio rarely got below 75 ppbv. If this value is defined as the initial and boundary conditions for CO, the model is expected to have a background value of about 75 ppbv over areas that are not affected significantly by continental sources. Since the model runs for only 17 days, calculated CO values tend to agree well with observations, particularly in areas remote from sources. Of course, the agreement is meaningless and the comparison is ineffective for testing the model performance. Other than increasing the model domain and running the model for a period of time comparable to the lifetime of CO, there is no satisfactory solution to this problem. A partial solution is to avoid the problem by comparing model results only for areas where CO levels are above the background value. In practice, one can subtract the background concentration of CO from the actual value and compare model results with observations for areas with large residuals only. In the following, we will mentally subtract 50 ppbv from all CO mixing ratios. This value is chosen to be less than 75 ppbv in order to account for the photochemical sink and stratospheric influence. For the other three species it is not practical to subtract a background value because of their short and/or variable lifetimes. For example, the photochemical lifetime of O_3 varies from a few days in the continental boundary layer to a few months in the upper troposphere [*Liu and Trainer*, 1988]. Thus its background level becomes altitude dependent and difficult to define.

3.1.1. Boundary layer. Plates 1a–1d show the latitude-longitude plots at 0.28 km altitude for model-simulated distributions of O_3, NO_y, SO_2, and CO, respectively. This altitude is the third vertical level from the bottom in the model and is representative of the boundary layer. As discussed above, values in these figures are averaged over the days (September 23 to October 6, 1991) of flights 6–13. For comparison, observed median values for individual segments during those flights are shown in numbers. The NO_y data are from the group of Georgia Institute of Technology for reasons discussed by *Crosley* [this issue]. The criterion for selecting a segment is that the aircraft stayed within the specified altitude range continuously

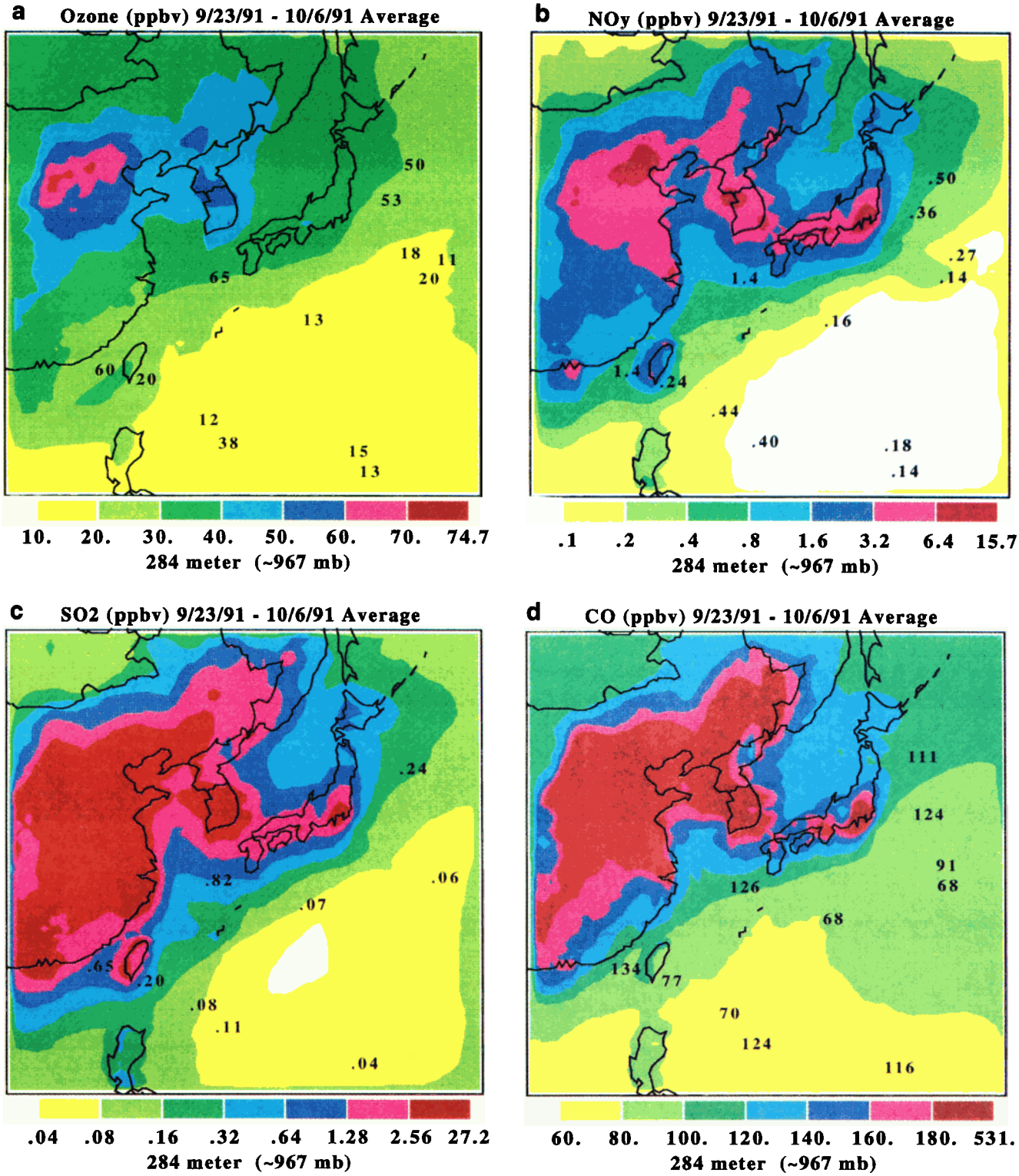

Plate 1. (a–d) Latitude-longitude plots for model-simulated distributions of O_3, NO_y, SO_2, and CO, respectively, at 0.28 km altitude (averaged over a time period from September 25 to October 6, 1991). Observed median values for individual segments below 0.5 km for flights 6–13 are shown in numbers.

for more than 10 min and there are more than five measurements of the species under consideration. In addition, observations during take-off and landing are excluded to avoid the influence of local emissions.

As expected, the most obvious feature of the model results in the boundary layer is a large decrease from continental areas toward the ocean in mixing ratios of all four species which have either major emissions (SO_2, CO, and NO_y) or significant photochemical production (O_3) in the continental planetary boundary layer (PBL). A second feature is that transport of trace species is preferentially toward the east and northeast due to the prevailing atmospheric circulation during this time

of the year, as discussed by *Bachmeier et al.* [this issue] and *Merrill* [this issue]. In addition, although there is obviously a significant transboundary transport of air pollutants, the emissions of individual countries and areas are discernible in the mixing ratio distributions in the PBL, particularly for primary pollutants like CO, NO_y, and SO_2 (Plates 1b, 1c, and 1d), suggesting that the levels of air pollutants in each country tend to be controlled by their own emissions.

The model results compare reasonably well with observed values both in general patterns and in absolute values. In particular, the observed mixing ratios of all four species show higher values along the northwestern edge of the area covered by flight tracks; this coincides well with the southeastern edge of the area with high model-calculated values, which is dominated by continental emissions. Values over the ocean to the southeastern part of the model domain tend to be uniformly low in both observed and in model-calculated trace species mixing ratios. The agreement in absolute values of SO_2 between model results and observations is remarkably good. However, the NO_y mixing ratio calculated by the model is below 100 pptv over a large area over the ocean (white color in Plate 1b), whereas the observed values are greater than 140 pptv. This may be due to the fact that the lightning source of NO_x has been omitted in the model. This will also give a lower ozone production and may contribute to the underestimate of ozone mixing ratios near the continent and Japan by the model. Another and probably more important contributor to the underestimate of ozone is due to the fact that the model results are averaged over about 2 weeks, while the observations are for a particular time. By examining the daily distributions of ozone, we noticed that there is a large fluctuation of the ozone mixing ratio with time, particularly near the continent where the plumes of pollutants have a sharp gradient. Furthermore, we have made a specific comparison of the high ozone value observed southwest of Japan (median value 65 ppbv) with model results for that day (October 6, 1991). The agreement is within 30%, much better than that shown in Plate 1a.

The agreement (or lack of agreement) between model results and observed absolute values of NO_y and SO_2 is particularly significant for testing the model's photochemistry and transport. As their lifetimes in the boundary layer are only about a few days, this will lead to a greater contrast in the concentrations between polluted and remote areas than long-lived species. In turn, the greater dynamic ranges in the concentrations of these species allow a more meaningful comparison between the model results and the observations.

There are some exceptionally high values in the observed mixing ratios that are not in agreement with the model results. They can be seen in the NO_y figure to the northeast of the Philippines where the median NO_y mixing ratio was observed at 0.44 and 0.4 ppbv, respectively. These values are 2 to 4 times higher than the model-calculated mixing ratios. The high value of 0.4 ppbv NO_y is accompanied by high values of O_3 (38 ppbv), SO_2 (0.11 ppbv), and CO (124 ppbv). Moreover, CO_2 and CH_4 mixing ratios were also high, suggesting either a combustion or a biomass burning source was responsible for these high levels of pollutants. Comparison of the observed ratios of trace species with emission inventories indicates that the latter is the most likely source. This is confirmed by trajectory analysis [*Merrill*, this issue] that shows the air mass originated from the Philippines where major biomass burning was occurring. The other high NO_y value (0.44 ppbv) is not accompanied by any increase in other trace species. Emissions from lightning are a likely source because it is not accompanied by any measurable high concentrations of other trace species. Since emissions from ships, lightning, and biomass burning are not included in the model calculations, it is not surprising to occasionally see that the calculated concentrations are significantly lower than those observed.

Abnormally high mixing ratios of CO (median at 116 pptv) were observed in the mid-Pacific at low latitudes. We are not able to find any explanation why the model underestimates the observed high CO median value of 116 ppbv at low latitudes or why it is not accompanied by any noticeable increase in other trace species.

In summary, there is a general agreement between distributions of trace species calculated by the model and observed values in the boundary layer. Furthermore, when there are disagreements, reasonable explanations are found for all cases, except one. This suggests that the model has the capability of simulating the major features of trace species within the boundary layer.

3.1.2. Upper troposphere. A similar comparison of model results with observations for the upper troposphere has been carried out. Plates 2a–2d show the latitude-longitude plots for model-simulated distributions of O_3, NO_y, SO_2, and CO, respectively, at an altitude of 11.15 km except for NO_y at 9 km. The 11.5 km altitude is the second vertical level and the 9 km altitude is third level below the top boundary of the model, which is near the tropopause. The lower altitude is chosen for NO_y because the optimal operational altitude for the NO_y instrument in the upper troposphere was below 11 km. Again as stated above, values in the figures are averaged over the days of flights 6–13. Observed median values for individual segments between 8 and 13 km of the flights are shown in numbers. The criteria for selecting the segments are the same as those for the boundary layer.

The most obvious pattern in the model results is an increase of mixing ratio from the southeast to the northwest for O_3, NO_y, and SO_2. This general pattern appears to be similar to that in the boundary layer. However, the cause of the pattern in the upper troposphere is completely different from that of the boundary layer. The former is due to the influence of a larger downward flux from the stratosphere in the northwestern region, whereas the latter is due to the influence of continental anthropogenic emissions that control the trace species distributions in the boundary layer.

Model-calculated distributions of O_3 and SO_2 are in good agreement with observed values both in the general pattern and in the absolute values. This is also the case for NO_y, except that model-calculated values are about 30 to 60% lower than those observed. An exception to the general pattern is the relatively low mixing ratios in all three species observed during Typhoon Mireille, which is obviously due to transport of low-altitude air by strong convective activities. This is also supported by relatively high mixing ratios of CO near southern Japan (113 and 120 ppbv) in Plate 2d as well as by observed high levels of DMS [*Newell et al.*, this issue]. To illustrate the effect of typhoons on the distribution of trace species, Plate 3 compares the model-calculated O_3 distribution to observed mixing ratios for the typhoon flight on September 27, 1991. Convective transport of boundary layer air to the upper troposphere has resulted in dramatically lower O_3 mixing ratios compared to the 14-day average values calculated by the model (Plate 2a).

Two other exceptions are the high NO_y mixing ratios in the

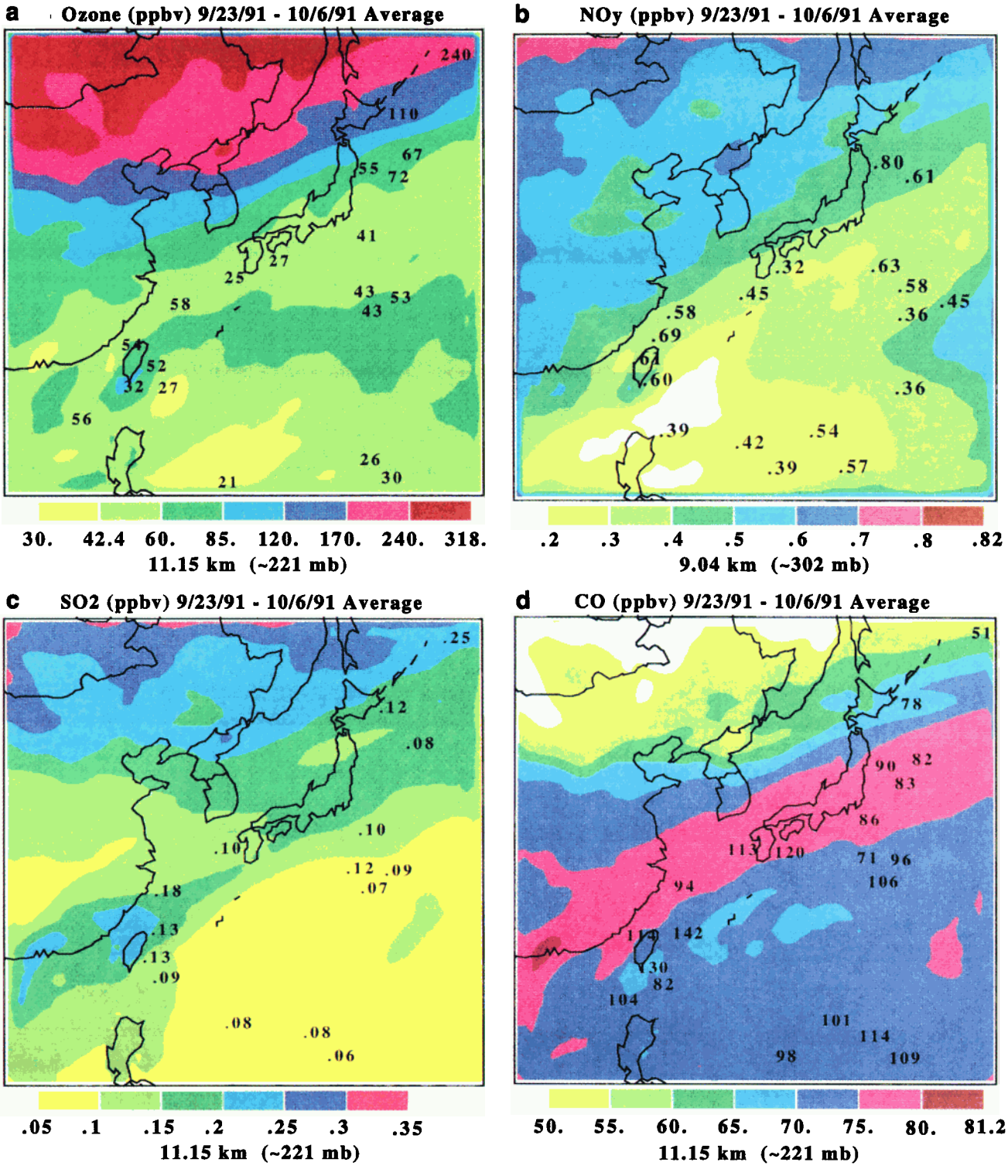

Plate 2. (a–d) Latitude-longitude plots for model-simulated distributions of O_3, NO_y, SO_2, and CO, respectively, at 11.15 km altitude except for NO_y at 9 km (averaged over a time period from September 25 to October 6, 1991). Observed median values for individual segments between 8 and 13 km for flights 6–13 are shown in numbers.

mid-Pacific (540 and 570 pptv) observed during two segments of flight 14 off the island of Guam. They are accompanied by relatively high CO readings (101 and 114 ppbv) and high NMHCs [*Blake et al.*, this issue], suggesting long-range transport of air pollutants as a likely source.

The general agreement between model results and observations for O_3 and SO_2 suggests that in the upper troposphere these two species are controlled by stratospheric sources. While this is not surprising for O_3, it is remarkable to see that stratospheric SO_2 from Mount Pinatubo emissions can account

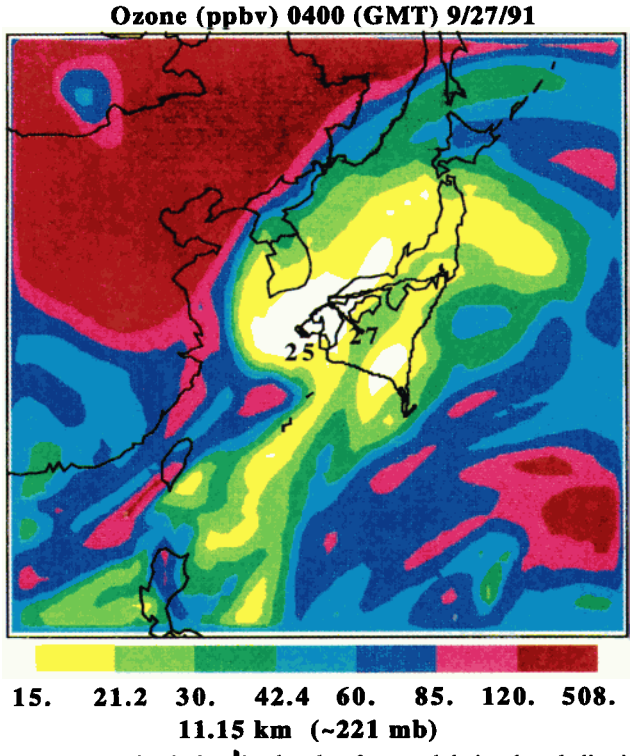

Plate 3. Latitude-longitude plot for model-simulated distributions of O_3 at 11.15 km altitude for September 27, 1991, when Typhoon Mireille was studied during flight 9. Observed median values for individual segments between 8 and 13 km for flight 9 are shown in numbers.

for most of the upper tropospheric SO_2. Thus the importance of the stratospheric intrusion to the upper tropospheric sulfur distribution three months after a major volcanic eruption is clearly demonstrated. This may have a significant implication for sulfur budget and formation of condensation nuclei in the upper troposphere [*Thornton et al.*, this issue].

For CO the model significantly underestimates its mixing ratio in most of the model domain. After subtracting the 50 ppbv background level, the observed values at some points are more than a factor of 2 higher than calculated CO mixing ratios. The only exception is in the northeastern region where the air mass clearly originates from the stratosphere [*Browell et al.*, this issue] and has the lowest median CO value (51 ppbv) during the entire PEM-West A experiment. This is simulated well by the model, which also gives a minimum near this point along the flight tracks. The model also underestimates the upper tropospheric concentrations of other trace species with similar characteristics of CO, i.e., with major sources in the continental boundary layer and sinks in the troposphere and stratosphere. All hydrocarbons fall into this category.

Apparently, the model simulates the upper troposphere distributions well for species which are controlled by stratospheric sources. This is also supported by a favorable comparison between model-calculated PV distributions in the upper troposphere and those derived from observations (not shown). Furthermore, *Browell et al.* [this issue] found extensive influence of stratospheric air throughout the upper troposphere, particularly at midlatitudes. As discussed in section 2, the initial and boundary conditions of O_3, SO_2, and NO_y are specified proportionally to PV in the upper five layers of the model. Given the high wind velocity in the upper troposphere, we believe that the model-calculated distributions of trace species above 5 km are controlled primarily by lateral boundary conditions (i.e., transport from upwind regions) [*Brost*, 1988; *McKeen et al.*, 1991] and transport from the stratosphere. Convective transport of trace species from the boundary layer to the upper troposphere can be substantial, but the model results indicate that significant convective transport occurs only in limited areas and/or special cases such as typhoons.

The above discussion suggests that underestimate of vertical transport and low mixing ratios specified for the upwind lateral boundary conditions (i.e., underestimate of the lateral transport from upwind regions) are two major reasons for the low mixing ratios of CO and hydrocarbons calculated by the model in the upper troposphere. They may also contribute to the low NO_y mixing ratios calculated by the model. However, the underestimate of NO_y may also be due to the absence of lightning and aircraft sources in the model.

It should be noted that the upwind lateral boundary conditions are controlled by emissions upwind of the model domain. This implies that a significant amount of trace species observed in the free troposphere during PEM-West A came from regions outside of eastern Asia. Analysis of the atmospheric transport and photochemical characteristics of continental trace gases by *Smyth et al.* [this issue] has reached a similar conclusion.

An underestimate of the vertical transport from the boundary layer to the upper troposphere also implies an underestimate of the transport of upper tropospheric air to the boundary layer. As a result, the model tends to overestimate the contribution of in situ sources (including stratospheric intrusions) to the upper tropospheric distribution of trace species. Previous studies [e.g., *Stauffer and Seaman*, 1991] indicate that the model makes an excellent simulation of the resolvable wind fields when FDDA is used (see also Figures 1a and 1b), suggesting that resolvable vertical transport is well simulated. The underestimate in vertical transport by the model must be due to subgrid processes, particularly transport by convective activities. At this moment, without an extensive modeling study, we are not able to evaluate quantitatively the effect of this model deficiency on the distributions of trace species in the upper troposphere for the PEM-West A period. A preliminary analysis of the observed distribution of SO_2 in the upper troposphere indicates the effect may be significant. This is probably a major source of uncertainty in this model study.

3.2. Budget of NO_y in the Upper Troposphere

The budget of upper tropospheric NO_y is an important subject of the tropospheric chemistry because of the role played by NO_y in the odd hydrogen photochemistry and the production of O_3, particularly from NO_x emitted by aircraft [*Liu et al.*, 1980; *Prather et al.*, 1992]. Results in section 4 have an important implication on the sources of upper tropospheric NO_y. For simplicity of argument, lets first assume that the model simulates the transport processes accurately. With only a stratospheric source of NO_y, calculated mixing ratios by the model in the upper troposphere agree well with observations in the general pattern and are only about a factor of 2 lower than observations in absolute values. This suggests strongly that the stratospheric source is an important contributor to upper tropospheric NO_y, consistent with an earlier study by *Kley et al.* [1981]. If this is true, one has to conclude that emissions from subsonic aircraft contribute at least as much as the stratospheric source to the upper tropospheric NO_y because the two

sources are comparable in source strength and both are upper tropospheric sources (see a review by *Fehsenfeld and Liu* [1993]). This means that the two sources can approximately account for all upper tropospheric NO_y.

The above conclusion leaves a puzzling question. Does this mean that the contribution by other NO_y sources to the upper tropospheric NO_y is negligible, especially the large sources in the continental boundary layer (about 30 Tg N per year [*Logan*, 1983]) and the lightning source? The answer must be yes for the boundary layer sources. Apparently, wet and dry removal of NO_y is efficient enough to prevent these sources from making a significant contribution in the upper troposphere. This is consistent with the findings of *Smyth et al.* [this issue] and *Singh et al.* [this issue]. The answer is more subtle for the lightning source because it has been proposed that a significant amount of NO_y from lightning can be transported into the stratosphere over the tropics and recycled back into the troposphere at higher latitudes [*Tuck*, 1976; *Kley et al.*, 1981; *Ko et al.*, 1986; *Murphy et al.*, 1993]. In other words, lightning NO_y source may contribute significantly to the stratospheric source represented by the ratio of NO_y to PV at the upper and lateral boundaries of the model. In this context there is also some contribution from subsonic aircraft since some of them fly above the tropopause. Quantitatively, according to the estimate of *Murphy et al.* [1993], NO_y from N_2O oxidation in the stratosphere contribute to at least half of the stratospheric source. Thus the N_2O source contributes to at least one quarter of the upper tropospheric NO_y. The source strengths of subsonic aircraft and stratospheric N_2O oxidation are about 0.7 and 0.5 Tg (N) per year, respectively [*Fehsenfeld and Liu*, 1993]. Since over 90% of the aircraft emissions occur in the northern hemisphere (NH), the ratio of the subsonic aircraft source to stratospheric N_2O source in the NH is about 2. Therefore the aircraft emissions should contribute to about one half of the NO_y in the upper troposphere. The rest (one quarter) is attributed to lightning and surface sources. This evaluation of the upper tropospheric NO_y budget is in basic agreement with an earlier study by *Kley et al.* [1981].

It is important to qualify, however, that the above conclusion is drawn under the assumption that the vertical transport is accurately simulated in the model. The contribution of surface sources to the upper tropospheric NO_y budget will increase with enhanced vertical transport. The model's underestimate of the vertical transport will lead to an underestimate of the importance of surface sources relative to upper tropospheric sources. Furthermore, the above study is limited to the upper troposphere over the western Pacific and is outside the tropical area. More observational and modeling studies are needed to evaluate the global budget of tropospheric NO_y, particularly in the tropics.

3.3. Continental Air Versus Marine Air

Major observed characteristics of continental air were compared to those of marine air by *Gregory et al.* [this issue] and *Talbot et al.* [this issue]. In these studies, classification of continental and marine air masses was made by back trajectory analysis for air masses along the flight trajectories [*Merrill*, this issue]. An air mass that passed over a continental area in the last five days or less was classified as continental air, while marine air was defined as an air mass that had not passed over any continental area in the last 10 days or longer. The authors compared the compositions between the two groups of air masses by plotting medians, quartiles, and ranges of trace species at various altitudes. Their plots for CO, C_2H_2, O_3, and NO_y are reproduced in Figures 2a–2d side by side with the corresponding plots from the model results.

Model results displayed in Figures 2a–2d are derived by following a similar classification of air masses used for observed data. However, because the model domain is smaller compared to the study area used by *Gregory et al.* [this issue] and *Talbot et al.* [this issue], 10-day back trajectories of air masses frequently reach beyond the boundaries of the model domain. To have enough data points, the time requirement of the marine air classification is reduced to 6 days the model results. This reduction in time requirement is not a problem, as it will become apparent later that the marine air defined above for the model has little contact with any continental air and has essentially the composition specified by the initial and boundary conditions over the ocean.

Another difference between the model's air mass classification and that of the observations is that the former determines back trajectories by following wind fields calculated by the model for grid points within the study area as indicated in Figure 1. To preserve self-consistency in the model's results, it is necessary to use the model's wind fields instead of the isentropic back trajectories analyzed by *Merrill* [this issue]. We do not expect that the difference in air mass classification would lead to any significant bias in the model results because the study areas overlap substantially with the flight tracks and model wind fields have been shown to be in good agreement with results of isentropic trajectory analysis [*Kuo et al.*, 1985].

As pointed out by *Gregory et al.* [this issue], difference in the altitude profiles between continental and marine air masses is an indicator of continental outflow for continentally emitted trace species like CO and C_2H_2. However, the difference alone does not give a measure of the flux of continental outflow. Additional information, namely, wind velocity and probability of occurrence of the continental air at each point, is needed to evaluate the flux. While the former can be obtained in the PEM-West data, the latter needs substantially more temporal and spatial coverage than is available from current observations. Nevertheless, comparisons of the altitude profiles calculated by the model with observed values can provide a valuable test of how well the model simulates the transport processes. In the following, the comparison is done for CO and C_2H_2. Several conclusions can be drawn from the comparison and they apply to both CO and C_2H_2. For simplicity we use CO as the surrogate for discussion and make comments on C_2H_2 only when there is a significant difference.

First, in the lower troposphere (below 7 km), both observations and model results show that CO and C_2H_2 mixing ratios of continental air are significantly higher than those of marine air. However, the difference in median values between continental air and marine air is about twice as large in the observations relative to the model calculations. Furthermore, the model results do not reproduce the positive altitude gradients for CO or C_2H_2 in the marine air due to the reasons stated in section 3.1.2, i.e., underestimate of the lateral transport from upwind regions and the vertical transport from the continental boundary layer. Thus while the model is successful in simulating a significant transport of the trace species emitted in the continental boundary layer to the Pacific, it appears to underestimate the flux. The difference in C_2H_2 profiles between the model and the observations is only about 30%. However, there are substantially fewer observations for C_2H_2 than CO and there is more scatter in the observed profile for the former.

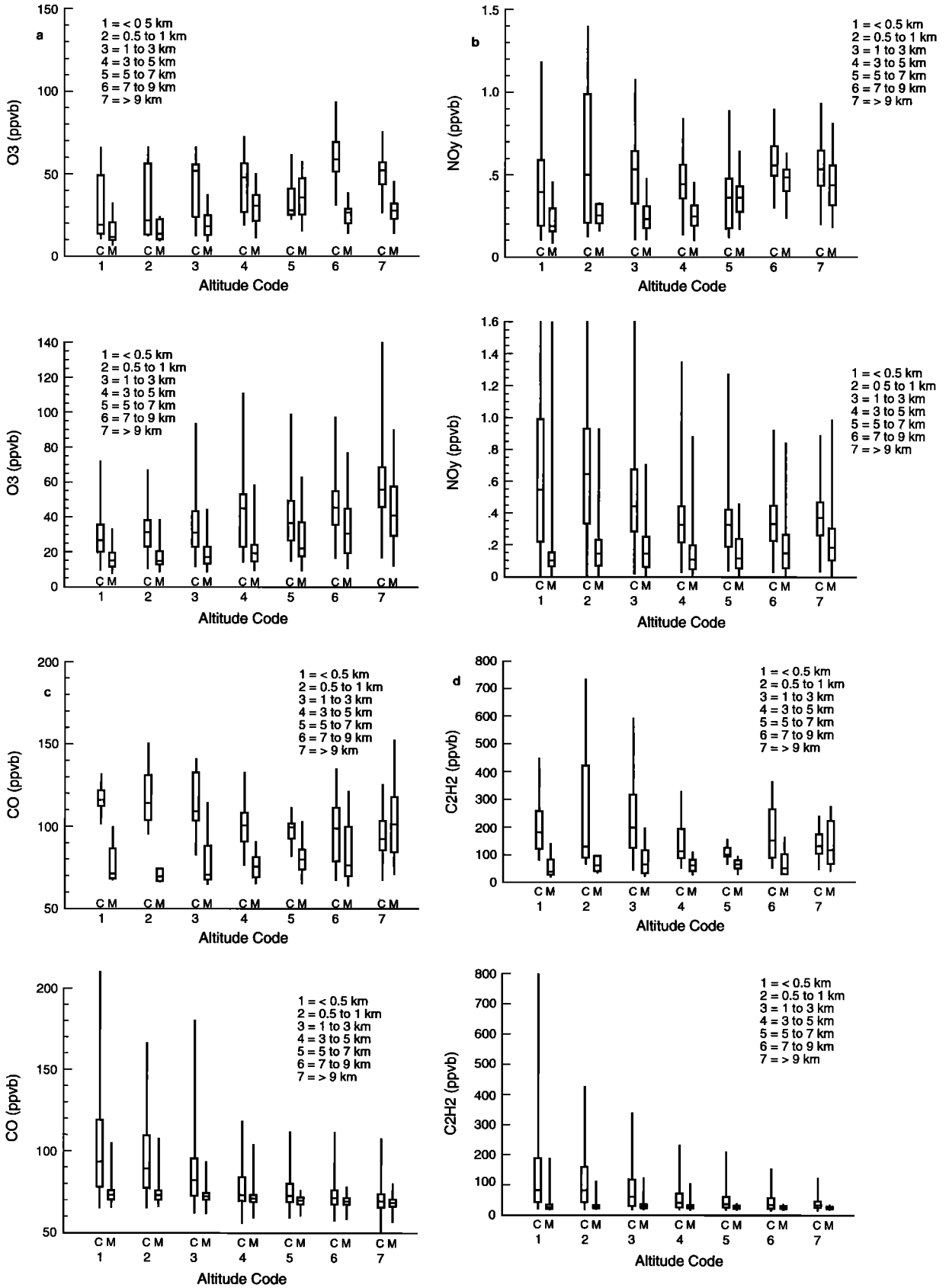

Figure 2. (a–d) Medians, quartiles, and ranges of O_3, NO_y, CO, and C_2H_2, respectively at various altitudes are plotted for continental air (denoted by C) and marine air (denoted by M). The top figures show observed values and lower figures are from model results.

Second, the quartiles and ranges of continental air below 7 km calculated by the model are in good agreement with observed values, again indicating that outflow from the continent in the lower troposphere is simulated reasonably well in the model. Meanwhile, we notice that observed values of the quartiles and ranges of marine air are substantially greater than values calculated by the model. This should not be construed as a model defect as much as the agreement in the median CO level of marine air is a model virtue because, as discussed earlier, the CO and C_2H_2 values of marine air in the model are determined primarily by boundary conditions, in other words, by transport of these gases from regions upwind of the model domain.

Third, both observations and model results show that the differences in CO as well as C_2H_2 levels between continental and marine air masses diminish in the upper troposphere. This suggests that direct influence of eastern Asian emissions via vertical transport processes from the surface to the free troposphere are largest in the lower troposphere and mostly limited to altitudes below 9 km, consistent with the conclusion reached by *Gregory et al.* [this issue]. Thus the CO distribution above 9 km must be controlled by long-range transport processes with scales greater than the model domain. However, this does not imply that globally the vertical flux from lower troposphere to 9 km and above is smaller than at lower altitudes. The flux can be larger, but horizontal transport and dispersion processes above 9 km are so fast that CO transported from below is mixed quickly and thoroughly so that little difference can be observed in the CO mixing ratio between continental and marine air masses.

Finally, in the marine air there is a positive altitude gradient in the observed CO mixing ratio. It is most evident when the highest layer (above 9 km) is compared to the lowest three layers (below 3 km). The positive altitude gradient exists also in the altitude profiles of O_3 and NO_y. In fact, the positive gradient in altitude profile is present in all trace species which are emitted over the continent. What is the cause(s) of the positive altitude gradient in the mixing ratio of a trace species in the marine air? Obviously, a stratospheric or upper tropospheric source can result in a positive gradient. This is evident in the positive gradient in marine air simulated by the model for O_3 and NO_y. For other species, a different process(es) must be responsible for the positive gradient. In a recent study of altitude distribution of nonmethane hydrocarbons, *Blake et al.* [1992] found similar positive gradients and suggested three different types of meteorological conditions that might contribute to the positive gradient in their data. All three included an efficient vertical convection process over continental source areas. Their differences were in the detailed transport mechanisms of the convection and what followed the convection. The first included a thoroughly mixed column of air at all altitude levels plus a greater photochemical sink in the lower altitude due to a higher OH concentration. The second required a faster horizontal transport in the upper troposphere than the lower troposphere so that the upper tropospheric air would be exposed to less reaction with OH. The third required a cloud pumping mechanism like the one proposed by *Gidel* [1983] that rapidly pumped boundary layer species up to and deposited them in the upper troposphere. *Blake et al.* [1992] did not indicate any preference but suggested a mixture of them. PEM-West A data have shed more light to this question. The fact that there is a negative altitude gradient for CO and C_2H_2 mixing ratios in the continental air (air over the ocean with continental origin) despite the higher OH concentration and slower wind velocity in the lower troposphere suggests that the third type is not the dominant mechanism because it would result in a positive vertical gradient for the continental air. Vertical transport or mixing from the surface to the lower and middle troposphere needs to be efficient enough to maintain the negative gradient in the continental air. However, because of the tendency of a faster horizontal dispersion of trace species in the upper troposphere due to stronger winds, we cannot determine the relative magnitude of vertical transport to various altitudes.

A mechanism that can explain the altitude gradients of CO and C_2H_2 for both continental air and marine air may be described as follows. When air masses pass over continental areas, they entrain boundary layer emissions through convection or other vertical transport processes. The entrainment as well as detrainment need to be significant at all altitudes. Furthermore, to obtain a negative gradient for the entrained trace species in the continental air, the entrainment must be large enough at lower altitudes to overcome the effect of a greater sink due to greater OH and smaller wind velocity. In other words, direct cloud pumping to the upper troposphere alone would not work. For the marine air, the positive gradient of trace species can be maintained by a combination of the following two processes: first, fast dispersion of CO and C_2H_2 transported to upper troposphere due to strong horizontal wind and turbulence, and second, greater OH concentration and lower wind velocity in the lower troposphere which results in air masses staying longer over the ocean in the lower troposphere than in the upper troposphere.

Observed NO_y and O_3 altitude profiles look similar to those of CO and C_2H_2 except that for continental air the negative altitude gradient found in CO and C_2H_2 is absent in NO_y and more so in O_3. In fact, the latter has a positive gradient. These features which are obviously due to stratospheric and/or upper tropospheric sources are simulated very well by the model, particularly for O_3. The model underestimates NO_y in the marine air by about 50%. As discussed in sections 2 and 3, this may likely be due to the omission of important free tropospheric sources such as lightning and aircraft emissions.

4. Summary and Conclusions

A three-dimensional mesoscale transport/photochemical model is used to study the transport and photochemical transformation of trace species over eastern Asia and the western Pacific for the period from September 20 to October 6, 1991, of PEM-West. Latitude-longitude distributions for a set of key species in the boundary layer and in the upper troposphere from model results have been compared to aircraft measurements. The influence of emissions from continental boundary layer that is evident in the observed trace species distributions within the boundary layer is reasonably well simulated by the model.

In the upper troposphere, species which have a significant source in the stratosphere are simulated well in the model. These species include O_3, NO_y, and SO_2, suggesting that the upper tropospheric abundance of these species are controlled to a large extent by stratospheric sources. In the case of SO_2 the stratospheric source is identified to be mostly from the Mount Pinatubo eruptions which occurred about three months before the PEM-West A mission.

Concentrations in the upper troposphere for species such as

CO and hydrocarbons which are emitted in the continental boundary layer and have a tropospheric sink are significantly underestimated by the model, indicating that vertical transport processes including convection may be underestimated in the model. In addition and probably more important, low mixing ratios specified for the boundary conditions which are controlled by sources upwind of the model domain also contribute to the underestimate by the model for species like CO in the upper troposphere. In the future, hemispheric scale model calculations will be carried out to study this question.

We have made an analysis of the contribution of various sources to the upper tropospheric NO_y over the western Pacific at midlatitudes. Assuming that the vertical transport is accurately simulated in the model, we estimate that stratospheric N_2O oxidation, subsonic aircraft, and the rest (lightning plus surface sources) contribute approximately 25, 50, and 25%, respectively. However, there is evidence indicating an underestimate of the vertical transport by the model that will lead to an underestimate of the contribution of surface sources to the upper tropospheric NO_y budget. This model deficiency in simulating the vertical transport is the major source of uncertainty in our analysis of the upper tropospheric NO_y budget. More observational and modeling studies are needed to quantify and to narrow down the uncertainty.

The model results are also grouped by back trajectories to study the contrast between compositions of marine and continental air masses and then compared to results of similar analyses applied to observations by *Gregory et al.* [this issue] and *Talbot et al.* [this issue]. The model-calculated altitude profiles of trace species of continental and marine air masses are found to be qualitatively consistent with observations. However, the difference in the median values of CO and hydrocarbons between continental air and marine air is underestimated by the model. This again is because the model neglects upwind sources and/or underestimates vertical transport over the continent. The latter would lead to an underestimate of the outflow fluxes of trace species from the Asian continent and the Pacific rim countries to the ocean.

Observed altitude profiles for species like CO and hydrocarbons show an interesting difference between continental and marine air masses, namely, a negative gradient in continental air and a positive gradient in marine air. A mechanism that can explain the altitude gradients has been proposed as follows: entrainment of boundary layer trace species at all altitude over the continent through convection and other vertical transport processes, fast dispersion of the trace species by strong horizontal wind and turbulence in the upper troposphere, greater OH concentration at lower altitude, and lower wind velocity in the lower troposphere which leads air masses to stay longer over the ocean than those in the upper troposphere.

Acknowledgments. This research was supported in part by the Atmospheric Chemistry Project of the Climate and Global Change Program of the National Oceanic and Atmospheric Administration and by the NASA Global Tropospheric Experiment. We appreciate all PEM-West A participants for their support and cooperation, particularly the effort of DC-8 flight and ground crew. In addition, we thank Brian Ridley and Michael Trainer for helpful discussions.

References

Anthes, R. A., E. Y. Hsie, and Y-H Kuo, Description of the Penn State/NCAR mesoscale model version 4 (MM4), *NCAR Tech. Note, NCAR/TN-282+STR*, 66 pp., Natl. Cent. for Atmos. Res., Boulder, Colo., 1987.

Bachmeier, A. S., R. E. Newell, M. C. Shipham, Y. Zhu, D. R. Blake, and E. V. Browell, PEM-West A: meteorological overview, *J. Geophys. Res.*, this issue.

Beekmann, M., G. Ancellet, and G. Megie, Climatology of tropospheric ozone in southern Europe and its relation to potential vorticity, *J. Geophys. Res.*, *99*, 12,841–12,853, 1994.

Blake, D. R., et al., Summertime measurements of selected nonmethane hydrocarbons in the Arctic and subarctic during the 1988 Arctic Boundary Layer Expedition (ABLE 3A), *J. Geophys. Res.*, *97*, 16,559–16,588, 1992.

Blake, D. R., T.-Y. Chen, T. W. Smith Jr., C. J.-L. Wang, O. W. Wingenter, N. J. Blake, F. S. Rowland, and E. W. Mayer, Three-dimensional distributions of nonmethane hydrocarbons and halocarbons over the northwestern Pacific during the 1991 Pacific Exploratory Mission (PEM West A), *J. Geophys. Res.*, this issue.

Brost, R. A., The sensitivity to input parameters of atmospheric concentrations simulated by a regional chemical model, *J. Geophys. Res.*, *93*, 2371–2387, 1988.

Browell, E. V., et al., Large-scale air mass characteristics observed over western Pacific during the summertime, *J. Geophys. Res.*, this issue.

Carroll, M. A., et al., Aircraft measurements of NO_x over the eastern Pacific and continental United States and implications for ozone production, *J. Geophys. Res.*, *95*, 10,205–10,234, 1990.

Crosley, D. R., NO_y Blue Ribbon panel, *J. Geophys. Res.*, this issue.

Dignon, J., NO_x and SO_2 emissions from fossil fuels: A global distribution, *Atmos. Environ.*, *26*(A), 1157–1163, 1992.

Ebel, A., H. Hass, H. Jakobs, M. Laube, M. Memmesheimer, and A. Oberreuter, Simulation of ozone intrusion caused by tropopause fold and cut-off low, *Atmos. Environ.*, *25*(A), 2131–2144, 1991.

Environmental Protection Agency (EPA), The 1985 NAPAP emissions inventory (version 2): Development of the annual data and modelers' tapes, *Tech. Rep. EPA-600/7/89-012a*, Natl. Tech. Inf. Serv., Springfield, VA., 1989.

Fehsenfeld, F. C., and S. C. Liu, Tropospheric ozone: Distribution and sources, in *Global Atmospheric Chemical Change*, pp. 169–231, edited by C. N. Hewitt and W. T. Sturges, Elsevier Science, New York, 1993.

Gidel, L. T., Cumulus cloud transport of transient tracers, *J. Geophys. Res.*, *88*, 6587–6599, 1983.

Gregory, G. L., et al., Chemical signatures of aged Pacific marine air: Mixed layer and free troposphere as measured during PEM-West A, *J. Geophys. Res.*, this issue.

Hoell, J. M. Jr., et al., Operational overview of NASA GTE/CITE 2 airborne instrument intercomparison: Nitrogen dioxide, nitric acid, and peroxyacetyl nitrate, *J. Geophys. Res.*, *95*, 10,047–10,054, 1990.

Hoell, J. M. Jr., et al., Pacific Exploratory Mission-West A (PEM-West A): September–October 1991, *J. Geophys. Res.*, this issue.

Hübler, G. H., D. W. Fahey, B. A. Ridley, G. L. Gregory, and F. C. Fehsenfeld, Airborne measurements of total reactive odd nitrogen (NO_y), *J. Geophys. Res.*, *97*, 9833–9850, 1992.

International Energy Agency (IEA), *Energy Balance of OECD Countries 1970/1985*, Organ. for Econ. Coop. and Dev./IEA, Paris, 1987.

Kato, N., and H. Akimoto, Anthropogenic emissions of SO_2 and NO_x in Asia: Emission inventories, *Atmos. Environ.*, *26*(A), 2997–3017, 1992.

Kley, D., J. W. Drummond, M. McFarland, and S. C. Liu, Tropospheric profiles of NO_x, *J. Geophys. Res.*, *86*, 3151–3161, 1981.

Ko, M. K. W., M. B. McElroy, D. K. Weisenstein, and N. D. Sze, Lightning: A possible source of stratospheric odd nitrogen, *J. Geophys. Res.*, *91*, 5395–5404, 1986.

Kuo, Y-H., M. Skumanich, P. L. Haagenson, and J. S. Chang, The accuracy of trajectory methods as revealed by the observing system simulation experiments, *Mon. Weather Rev.*, *113*, 1852–1867, 1985.

Lamb, B., A. Guenther, D. Gay, and H. Westberg, A national inventory of biogenic emissions, *Atmos. Environ.*, *21*, 1695–1705, 1987.

Lin, X., B. A. Ridley, J. Walega, G. F. Hübler, S. A. McKeen, E.-Y. Hsie, M. Trainer, F. C. Fehsenfeld, and S. C. Liu, A parameterization of subgrid scale convective cloud transport in a mesoscale regional chemistry model, *J. Geophys. Res.*, *99*, 25,615–25,630, 1994.

Liu, S. C., and M. Trainer, Responses of tropospheric ozone and odd hydrogen radicals to column ozone change, *J. Atmos. Chem.*, *6*, 221–233, 1988.

Liu, S. C., D. Kley, M. McFarland, J. D. Mahlman, and H. Levy, II, On

the origin of tropospheric ozone, *J. Geophys. Res.*, *85*, 7546–7552, 1980.

Logan, J. A., Nitrogen oxides in the troposphere: Global and regional budgets, *J. Geophys. Res.*, *88*, 10,785–10,807, 1983.

Lurmann, F. W., A. C. Lloyd, and R. Atkinson, A chemical mechanism for use in long-range transport/acid deposition computer modeling, *J. Geophys. Res.*, *91*, 10,905–10,936, 1986.

McKeen, S. A., E. Y. Hsie, M. Trainer, R. Tallamraju, and S. C. Liu, A regional model study of the ozone budget in the eastern United States, *J. Geophys. Res.*, *96*, 10,809–10,846, 1991.

McKeen, S. A., et al., Hydrocarbon ratios during PEM-West A: A model perspective, *J. Geophys. Res.*, this issue.

Merrill, J. T., Trajectory results and interpretation for PEM-West A, *J. Geophys. Res.*, this issue.

Murphy, D. M., D. W. Fahey, M. H. Proffitt, S. C. Liu, C. S. Eubank, S. R. Kawa, and K. K. Kelly, Reactive nitrogen and its correlation with ozone in the lower stratosphere and upper troposphere, *J. Geophys. Res.*, *98*, 8751–8774, 1993.

Newell, R. E., et al., Atmospheric sampling of supertyphoon Mireille with the NASA DC-8 aircraft on September 27, 1991, during PEM-West, *J. Geophys. Res.*, this issue.

Organization for Economic Cooperation and Development/International Energy Agency, (OECD/IEA), *World Energy Statistics and Balances 1985–1988*, Paris, 1990.

Piccot, S. D., J. L. Watson, and J. Jones, A global inventory of volatile organic compound emissions from anthropogenic sources, *J. Geophys. Res.*, *97*, 9897–9912, 1992.

Prather, M. J., et al., The atmospheric effects of stratospheric aircraft: A first program report, *NASA Ref. Publ. 1272*, 1992.

Ridley, B. A., et al., Ratios of peroxyacetyl nitrate to active nitrogen observed during aircraft flights over the eastern Pacific oceans and continental United States, *J. Geophys. Res.*, *95*, 10,179–10,192, 1990.

Singh, H., et al., Reactive nitrogen and ozone over the western Pacific: Distribution, partitioning, and sources, *J. Geophys. Res.*, this issue.

Smyth, S., et al., Comparison of free-tropospheric western Pacific air mass classification schemes for the PEM-West experiment, *J. Geophys. Res.*, this issue.

State Statistical Bureau of China (SSBC), *The Yearbook of Energy Statistics of China 1989* (in Chinese), China Stat. Publ. House, Beijing, 1990.

Stauffer, D. R., N. Seaman, and F. S. Binkowski, Use of four-dimensional data assimilation in a limited-area mesoscale model, II, Effects of data assimilation within the planetary boundary layer, *Mon. Weather Rev.*, *119*, 734–754, 1991.

Talbot, R. W., et al., Chemical characteristics of continental outflow from Asia to the troposphere over the western Pacific Ocean during September–October 1991, Results from PEM-West A, *J. Geophys. Res.*, this issue.

Thornton, D., A. R. Bandy, B. W. Blomquist, D. D. Davis, and R. W. Talbot, Sulfur dioxide as a source of CN in the upper troposphere of the Pacific Ocean, *J. Geophys. Res.*, this issue.

Tuck, A. F., Production of nitrogen oxides by lightning discharges, *Q. J. R. Meteorol. Soc.*, *102*, 749–755, 1976.

Williams, E. J., A. Guenther, and F. C. Fehsenfeld, An inventory of nitric oxide emissions from soils in the United States, *J. Geophys. Res.*, *97*, 7511–7520, 1992.

A. R. Bandy and D. C. Thornton, Drexel University, Philadelphia, PA 19104.

D. R. Blake and F. S. Rowland, University of California, Irvine, CA 92717.

J. D. Bradshaw and S. T. Sandholm, Georgia Institute of Technology, Atlanta, GA 30332.

E. V. Browell, G. L. Gregory, and G. W. Sachse, NASA Langley Research Center, Hampton, VA 23665.

B. G. Heikes, University of Rhode Island, Narragansett, RI 02882.

E. Y. Hsie, X. Lin, and A. S. McKeen, Cooperative Institute for Research in Environmental Sciences, University of Colorado, Boulder, CO 80309.

K. K. Kelly and S. Liu (corresponding author), Aeronomy Laboratory/NOAA, Boulder, CO 80303.

R. Newell, MIT, Cambridge, MA 02139.

H. Singh, NASA Ames Research Center, Moffett Field, CA 94035.

R. W. Talbot, University of New Hampshire, Durham, NH 03824.

(Received September 9, 1994; revised June 24, 1995;
accepted June 24, 1995.)